Chapter 6

Field data results

6.1 DESCRIPTION OF THE DATA

The salt data set is part of a seismic survey in the deep Gulf of Mexico, consisting of 1400 shots with a spacing of 26.8 m (88 feet). The cable has 180 geophones that are also 26.8 m apart; the near-offset distance is 193.8 m. Thus, the total cable length is nearly 5 km, which is longer than cable lengths typically used in marine seismic surveys. Large offsets are required to get wide-angle coverage over the deep sediments. Likewise, recording time is longer than usual: 11 s at a sample rate of 2 ms. The line is shot in the regional dip direction.

Arco's preprocessing of the data includes deconvolution and water-bottom-multiple elimination. Water-bottom multiples are dominant in the original data, but their moveout is sufficiently different from the primary moveout that they can be removed efficiently. At near offsets, where this moveout distinction is less clear, the multiple-elimination filter also removes part of the primary energy, as can be seen in Figure 2.1. I applied a simple AGC filter to the data to correct for amplitude variations caused by the preprocessing.

A distinct feature in this data set is the "ringing" of the salt top reflection (Figures 2.3 and 2.4). Careful examination of the shot gathers reveals that the salt is not homogeneous, but has a "cap" that generates a second reflection, which arrives just after the salt top reflection. Furthermore, peg-leg multiples of these reflection events (the short path of which are in the sediment layer above the salt) create two additional events. The ringing effect is typical for salt data recorded in this area (B. Verwest, Arco Oil and Gas Co., pers. comm.).

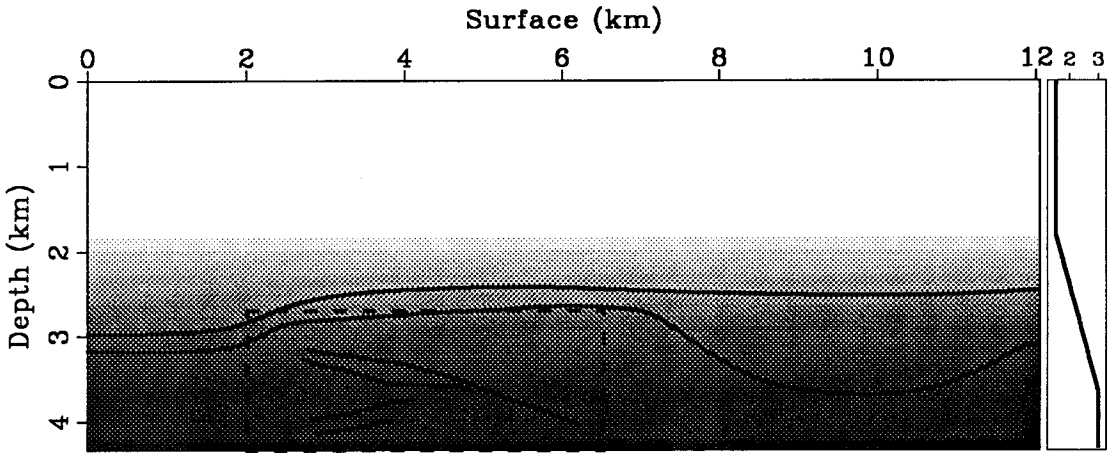

FIG. 6.1. Initial velocity model. The model is laterally invariant, and velocity increases from 1.5 km/s at the top to 3 km/s at the bottom (a depth profile is shown on the right-hand side of the figure). Low intensities denote low velocities. As a reference, the fat lines show the major near-offset reflectors. Velocities are estimated in the rectangular area denoted by the dashed box.

6.2 INVERSION RESULTS

The initial velocity model used for migrating the data is laterally invariant (Figure 6.1), and is found from averaging velocity profiles determined by NMO-velocity analysis of a few CMP gathers alongside the salt body. I already discussed the migrated data and their interpretation in Chapter 2 (sections 2.3.1 and 2.3.2), in which I showed that the largest residual moveout occurs below the salt structure. Therefore, I limit the velocity inversion to a small region in and below the salt body (the rectangular area in Figure 6.1). This region does not include the right-hand side of the salt body; there are no coherent reflectors below the salt in this part of the data that can be used for velocity analysis. As a reminder, the picked near-offset reflectors (Figure 2.7) are plotted on top of Figure 6.1. The inverted region is still of considerable size; the shot gathers included in the inversion extend over a surface range of about 10 km. Note that the finite-difference traveltime calculations are well-suited for this target-oriented inversion: only windows of the traveltime maps corresponding to the target region have to be kept in memory (or stored on disk) during the event migration and velocity optimization.

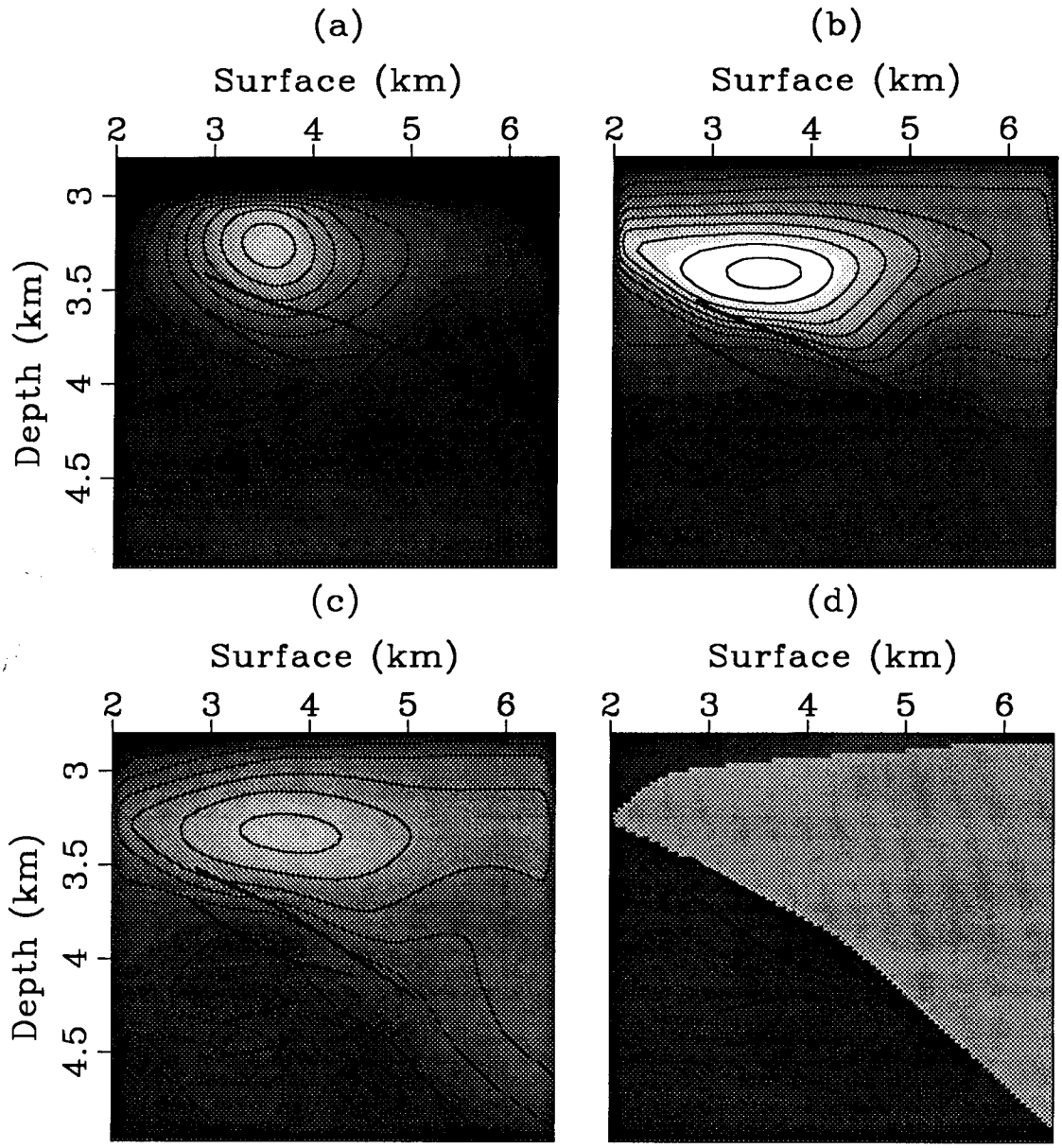

FIG. 6.2. Inversion results after 1 (a), 2 (b), and 3 nonlinear iterations (c). Figure (d) shows a window of the structural model of Figure 6.9. Low intensities denote high velocities (the intensity scale is the same for all plots); contours are drawn at .2 km/s intervals. The fat lines show the position of the near-offset reflectors after migration with the respective velocity models. Vertical exaggeration is 2:1.

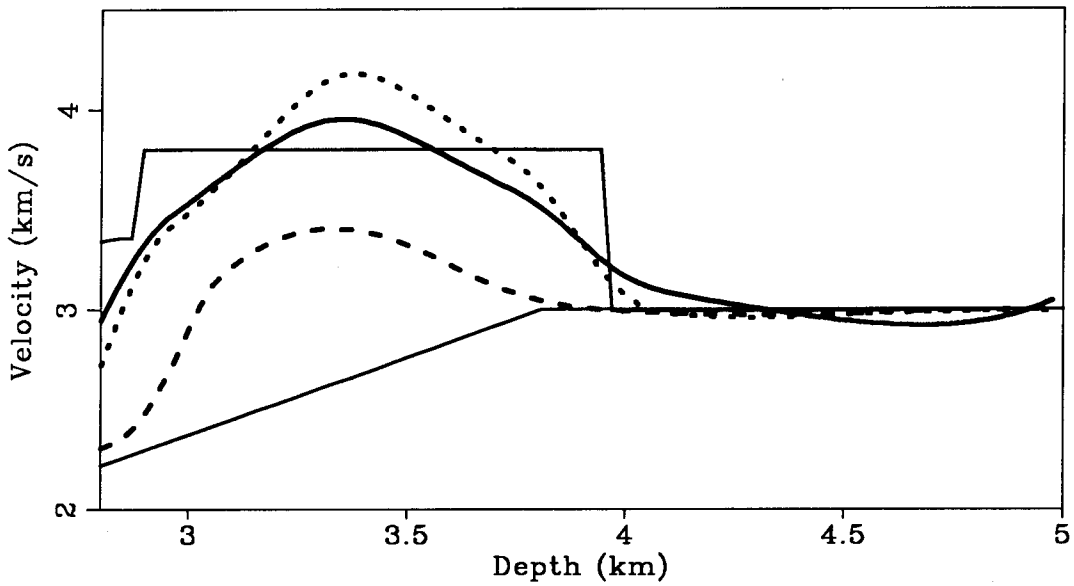

FIG. 6.3. Velocity profiles at a surface location of 4.5 km. The fat lines show the inversion results after 1 (dashed), 2 (dotted) and 3 iterations (solid). The thin, solid lines show the initial and structural model, respectively.

Figures 6.2 and 6.3 show the velocity-estimation results. The spline cells that I use in the model parametrization have a horizontal width of .4 km and a vertical one of .2 km. After 3 nonlinear iterations in the inversion (Figures 6.2a-c), the optimization achieves its goal of aligning the major reflectors in the different constant-offset sections (Figure 6.4b).

I use a diagonal damping matrix in the inversion; a completely unconstrained inversion tends to overcorrect velocities in spline cells that have the most influence on residual moveout. That is, although the optimization succeeds in reducing residual moveout, inverted velocities are too high in the central part of the salt, and too low at the salt edges. An indication of this bias can be seen in Figure 6.2a, which shows that the inversion initially puts a high-velocity blob in the middle of the salt region. Damping the optimization constrains the velocities such that additional iterations are able to "smooth out" the blob, as can be seen in Figures 6.2b and c. I choose the values of the damping constants by running some trial optimizations, which is feasible given the small computational cost of the inversion (one nonlinear iteration, which includes the calculation of traveltime maps at 500 surface locations, takes about 20 minutes of CPU on the Convex C-1).

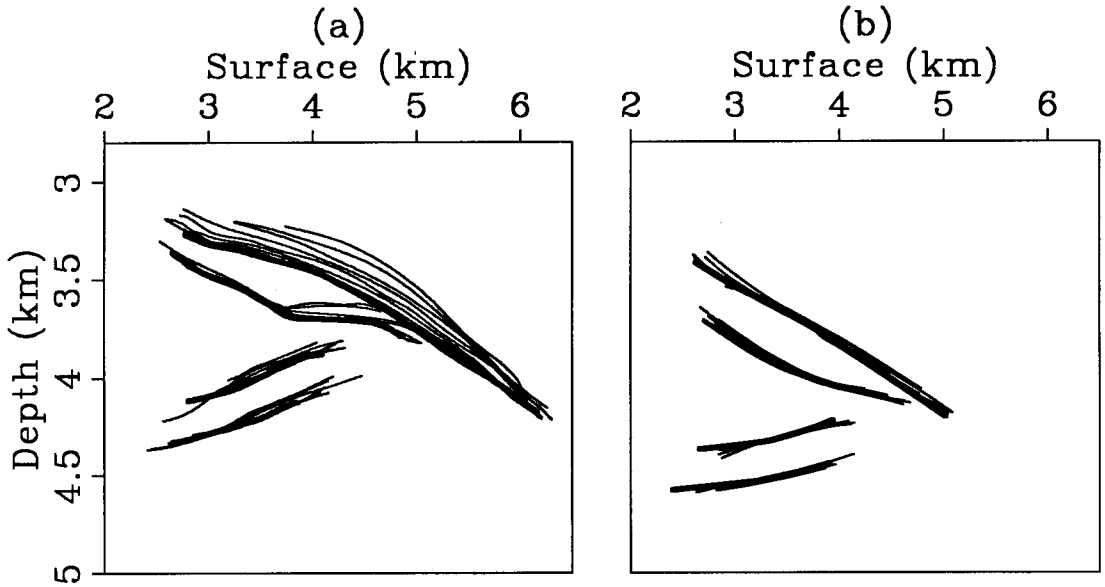

FIG. 6.4. Reflectors in the migrated constant-offset sections: (a) initial picks (the figure displays a window of Figure 2.7), and final position after inversion (b). The fat lines show the near-offset reflectors.

6.2.1 Residual moveout after inversion

Figure 6.5 shows several CRP gathers after migration with both the initial and the final model. Residual moveout in the gathers migrated with the final model is generally small, but event definition remains poor in some areas below the salt, mainly because sediments along the salt flank are fractured and faulted. Note that there is not a one-to-one correspondence between all the events in the initial and final gathers; events move laterally as well as vertically after residual migration, and they may therefore move to different surface locations. Although the previously mentioned peg-leg multiples do not distort the velocity analysis, they have some unwanted effects on the imaging. The moveout of the multiples is determined by sediment velocity, and, after migration with the much higher salt velocity, they are curving downward and interfere with primary events at large offsets. Therefore, I mute the prestack migrated data to avoid artifacts in the stacked image (see Figure 6.5).

Remigration of the full data set is not necessary in the velocity estimation; remigration is performed here only to test the inversion results. Nevertheless, after each nonlinear iteration, I normally remigrate a few constant-offset sections with the updated velocity model to confirm that residually migrated events still match events in the seismic data. This

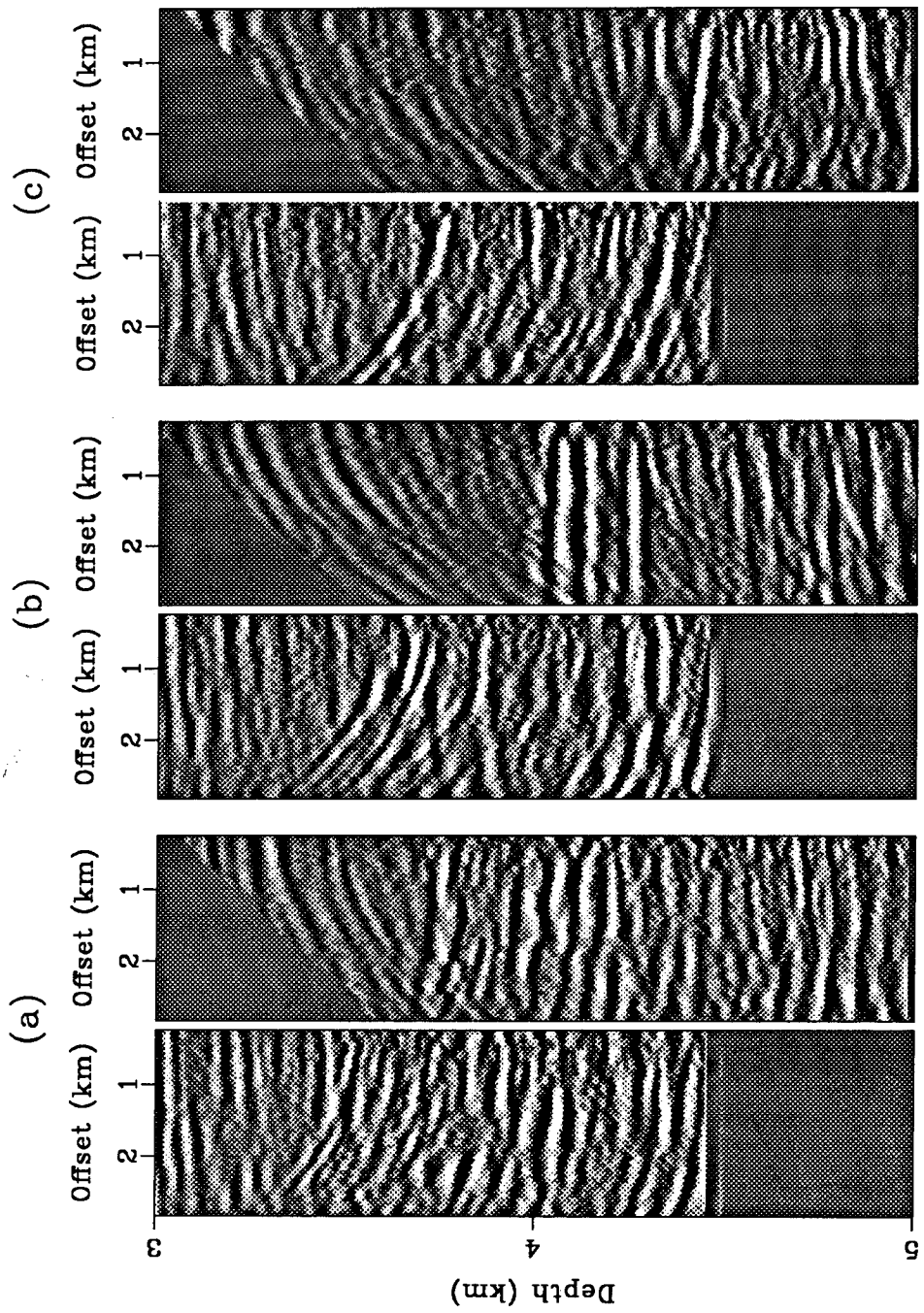

FIG. 6.5. Pairs of CRP gathers at surface locations of (a) 4, (b) 4.5, and (c) 5 km. The left gather in each pair is migrated with the initial model; the right one is found after migration with the final inverted model (Figure 6.2c). I display only inner offsets; at offsets larger than 3 km, little seismic energy penetrates the salt. The downward-curving events at the top of the right-hand gathers are peg-leg multiples of the salt top reflection. I mute out these events at large offsets to avoid artifacts in the stacked image.

procedure allows me to correct or re-interpret initial picks. Because Kirchhoff migration allows partial imaging of the subsurface, the re-imaging of the data can be limited to a few selected target zones around the major events, and is therefore not computationally expensive.

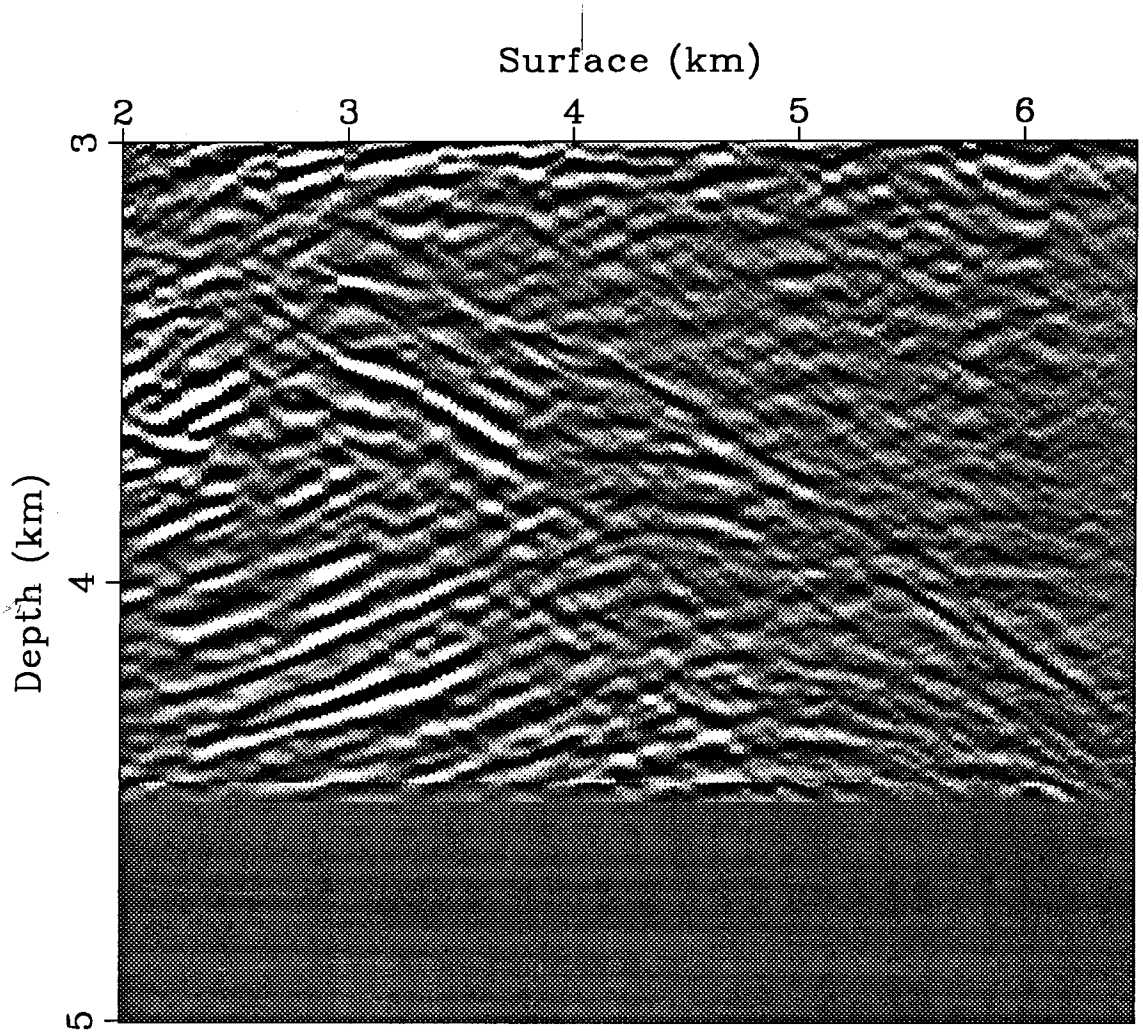

FIG. 6.6. Depth image of area below the salt after migration with initial velocity model (Figure 6.1). Vertical exaggeration is 2:1.

6.2.2 Imaging below the salt

Figure 6.7 shows the depth image of the area below the salt after migration with the final inverted velocity model. The image is considerably different from the initial one

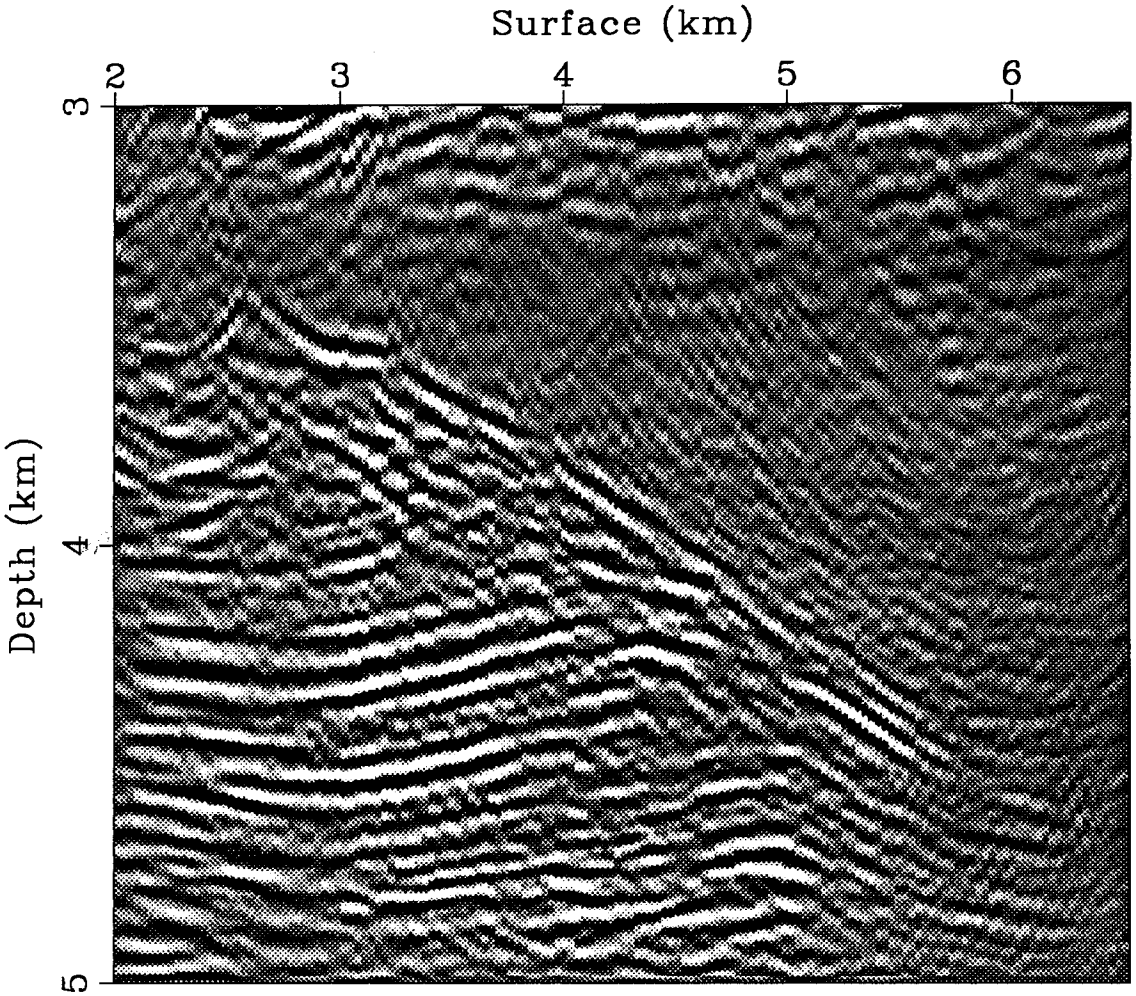

FIG. 6.7. Depth image of area below the salt after migration with the inverted velocity model (Figure 6.2c). Vertical exaggeration is 2:1.

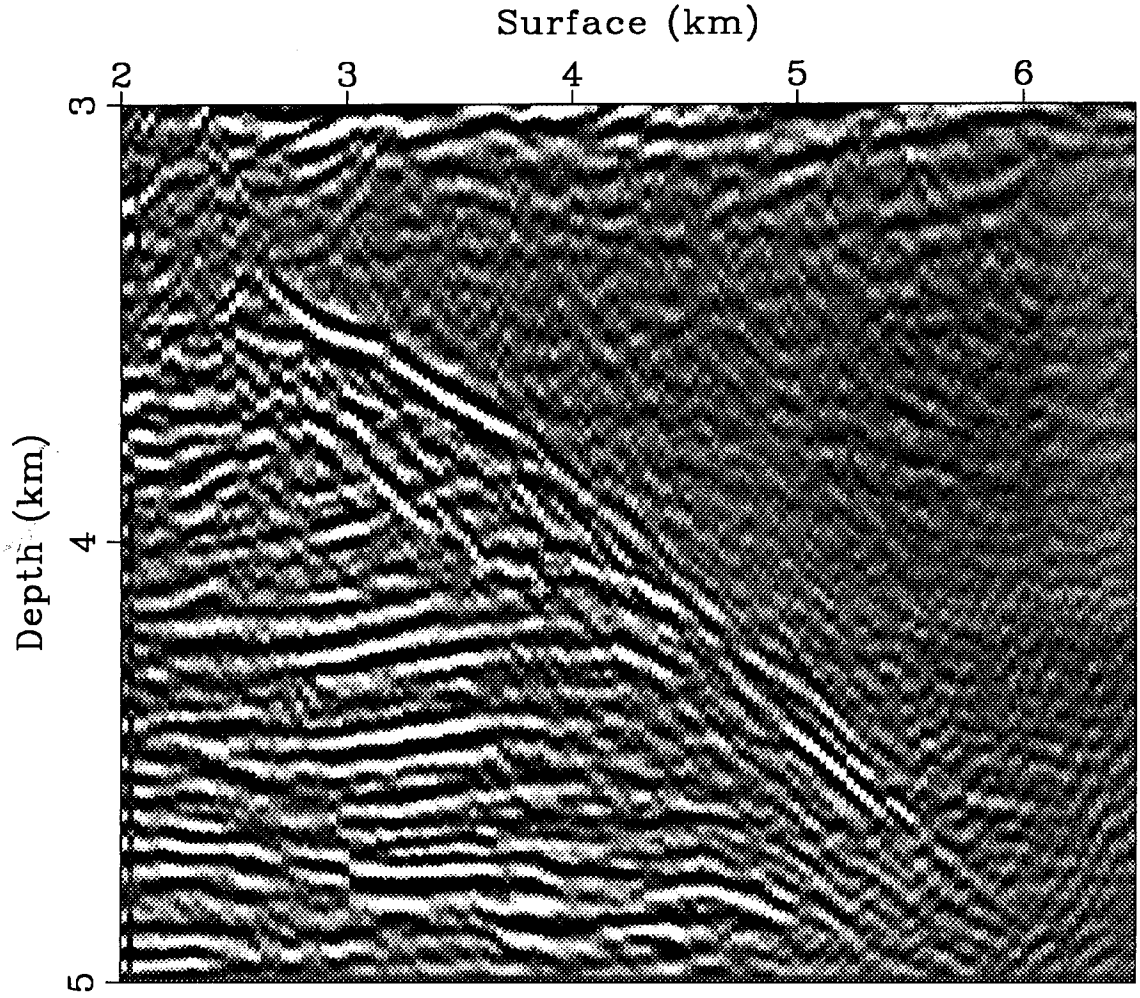

FIG. 6.8. Depth image of area below the salt after migration with the structural velocity model (Figure 6.9). Vertical exaggeration is 2:1.

(Figure 6.6): the salt boundary is properly imaged at the sediment truncations, and, most notably, the sediments below the salt are more continuous and much flatter than they are in the initial image. Although distinctly present in several prestack migrated sections (see for example Figure 4.7), the fault is not clearly visible in the final image. The fault reflection is weak, and not always present at all surface locations and offsets; its energy in the stacked image is low compared to that of the surrounding sediments.

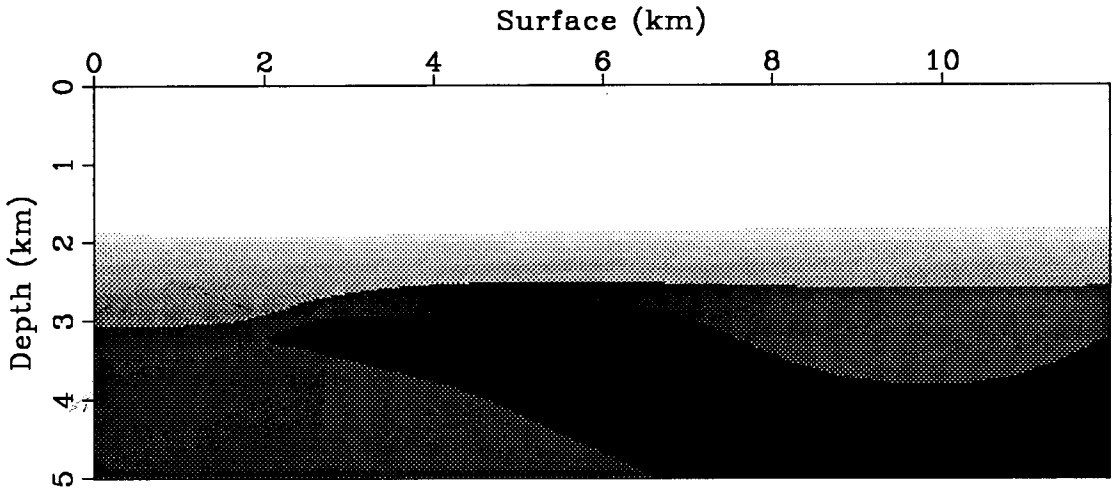

FIG. 6.9. Structural model. The salt bottom in the model is determined from depth image in Figure 6.7. Salt velocity is set to the velocity measured from waves refracting off of the salt top.

6.2.3 Structural model

Although the inversion achieves its goal of removing residual moveout in the prestack migrated data, and improves the seismic image of sediments below the salt, the inverted velocity model does not represent the structural shape of the salt body, simply because such a representation cannot be accomplished by a smooth 2-D spline function. Also, so far I have ignored velocity information from refracted events in the data.

Therefore, as a final test, I migrate the data with a structural model (Figure 6.9 and Figure 6.2d), which I construct from the migrated image discussed in the previous section (Figure 6.7). The salt velocity in the structural model is 3.8 km/s, and is calculated from the linear moveout of waves refracting off of the salt top. This velocity corresponds well

with the salt velocity estimated in the optimization (Figure 6.3). The velocities in the other structures are found by averaging inverted velocities over each structural region.

A migration of the data with the structural model will prove or disprove the inversion results: because the model has to be consistent with the seismic data, boundaries in the migrated image have to match structural boundaries. Figure 6.8 shows the image after migration of the data with the structural model. The salt bottom in the image indeed agrees with the bottom of the salt in the structural model (Figure 6.2d). Some discrepancies are apparent at the right-hand side of the salt bottom. At the edges of the model, the limited ray coverage prevents the inversion from recovering the full salt velocity, and thus the final image (Figure 6.7)—from which boundaries in the structural model are derived— is slightly inaccurate at the edges. (This can also be seen in Figure 6.5c, which shows that the salt bottom reflection still has some residual moveout after inversion.)

6.3 CONCLUSIONS

The velocity-estimation method succeeds in reducing residual moveout in the migrated data. Although the inversion does not directly produce a structural velocity model, it does find accurate reflector positions, which can then be used to build a structural model. Velocities in the structural model can be determined simply by averaging inverted velocities. Alternatively, they can be obtained from geological information, from well logs, or, as I have done here for salt velocity, from refraction events in the seismic data. A migration of the data with the structural model yields a depth image that is consistent with the inverted position of the major reflectors.

The final image of the area below the salt (Figure 6.8) is quite different from the initial one (Figure 6.6). The final image shows flat sediments below the salt, whereas sediments seem to bend upwards against the salt body in the initial image. Interpretations based on the two images may therefore draw widely differing conclusions; the field data example proves the importance of 2-D velocity analysis and depth migration in areas with complex structure and strong lateral velocity variation.